

Effect of Fiber Orientation and Ply Mix on Fiber Reinforced Polymer-Confined Concrete

Ching Au, A.M.ASCE,¹ and Oral Buyukozturk, M.ASCE²

Abstract: This paper explores the effects of fiber orientation and ply mix on load–deformation behavior and failure modes of fiber reinforced polymer (FRP) confined concrete by testing under uniaxial compression a designed array of plain concrete cylinders wrapped with different fabric orientation. Depending on the jacket confinement stiffness, either a strain hardening or a strain softening behavior was observed beyond the kink point where there was a sharp reduction in slope in the load–deformation curve. Kinking was seen to have a definable graphical relationship with the critical concrete lateral strain while the kink stress was found to upshift with increasing jacket stiffness. It is concluded that while hoop fiber wrapped concrete leads to brittle failures, angular fiber wrapped concrete tends to fail in a ductile manner, attributed to a fiber reorientation mechanism. Ply mix sequence plays an important role in the overall deformation and failure behavior. Existing models are found to be adequate in describing load–deformation behavior of angular fiber wrapped concrete as long as equivalent FRP properties in the hoop direction are used.

DOI: 10.1061/(ASCE)1090-0268(2005)9:5(397)

CE Database subject headings: Columns; Jacketing; Confinement; Fiber reinforced polymers; Concrete; Failure modes.

Introduction

Column retrofit using fiber reinforced polymer (FRP) jacketing has been extensively studied in the past decade to explore the effectiveness of this method in strength and ductility enhancement (Saadatmanesh et al. 1994; Nanni and Bradford 1995; Mirmiran et al. 1996, 1998; Mirmiran and Shahawy 1997a, b; Watanabe et al. 1997; Miyauchi et al. 1999; Lam and Teng 2000) while a large number of projects, both public and private have made use of such technology, especially in seismically active regions (Fyfe 2000). Yet, most of these studies and applications have focused on the use of fibers only in the hoop direction due to the anticipated strength increase and ease of application. Although some studies have been conducted on the use of angular fibers (Karbhari et al. 1993, Howie and Karbhari 1995; Mirmiran et al. 1996; Picher et al. 1996; Hoppel and Bogetti 1997), and it has been pointed out that the use of angular fibers could possibly improve failure mode (Howie and Karbhari 1995), the effects of fiber orientation and stack sequence are generally not well understood. Also, extensive efforts have been made to develop ultimate strength models for FRP wrapped columns (Lam and Teng 2000), but the structural significance of the ultimate state in terms of design and safety might not be as critical as that of the kinking point where there is a sharp reduction in slope in the load–deformation curve at about

where the unconfined concrete exhibits failure (Howie and Karbhari 1995).

The objective of this study is to explore the use of different fiber orientation and mix of ply configurations in attaining a range of load–deformation behavior and failure modes, from which improved physical insights into kinking phenomenon, fiber response, and ply interactions can be gained as a basis for behavioral enhancement for strength as well as ductility at failure of these systems. Experimental results are compared to existing stress–strain models for assessing their performance in quantifying the load–deformation behavior of cylindrical concrete passively confined by various angular fiber wrap configurations.

Experimental Work

Specimens

A total of 24 150 mm × 375 mm concrete cylindrical specimens were tested, of which 18 were FRP-wrapped while six were unwrapped control specimens. The 375 mm cylinder height was chosen based on the reported phenomenon that three-dimensional stress states would extend from the end surface to a distance of about 0.86 times the diameter of the cylinder (van Mier 1984) resulting from the elastic mismatch between the steel loading platens and the concrete cylinder. Thus for this research, cylindrical specimens with an aspect ratio of 2.5 were chosen so that an approximately 120 mm zone of the specimens at mid-height would be under uniaxial compression and free from three-dimensional stress effects from the ends. Concrete cylinders were vertically cast and had an average 28 day characteristic compressive strength of 24.2 MPa with a standard deviation of 2.2 MPa (150 mm × 375 mm cylinders).

The FRP fabrics made of E-glass fibers, impregnated in an ambient-cured two-part epoxy matrix, that were obtained from a United States manufacturer as commercially available systems,

¹Graduate Student, Dept. of Civil and Environmental Engineering, Massachusetts Institute of Technology, Cambridge, MA 02139.

²Professor, Dept. of Civil and Environmental Engineering, Massachusetts Institute of Technology, Cambridge, MA 02139 (corresponding author). E-mail: obuyuk@mit.edu

Note. Discussion open until March 1, 2006. Separate discussions must be submitted for individual papers. To extend the closing date by one month, a written request must be filed with the ASCE Managing Editor. The manuscript for this paper was submitted for review and possible publication on July 13, 2004; approved on March 14, 2005. This paper is part of the *Journal of Composites for Construction*, Vol. 9, No. 5, October 1, 2005. ©ASCE, ISSN 1090-0268/2005/5-397–407/\$25.00.

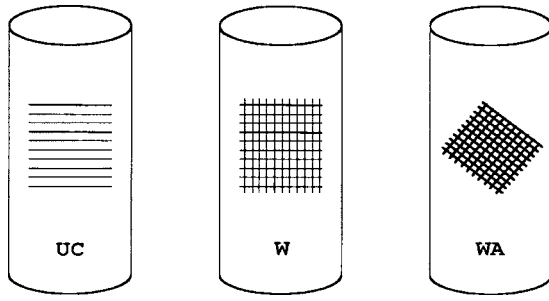


Fig. 1. Basic fabric designation

were used throughout this study. Three types of fabrics were employed to produce six wrap configurations. Designations for 0° hoop, 0°/90° hoop/vertical, and ±45° biangular fabrics were, respectively, UC, W, and WA, as illustrated in Fig. 1. The UC fabric consisted of unidirectional fiber roving densely placed in the 0° direction with additional sparsely spaced glass fibers in the 90° direction for linking purposes. The W fabrics consisted of 0°/90° bidirectional weaved fibers with equal fiber content running in both directions. The WA fabrics also consisted of bidirectional weaved fibers with equal fiber content in both directions but they were oriented in ±45°. Respective tensile properties and laminate thickness are summarized in Table 1.

The ambient-cured two-part epoxy had a tensile strength of 72.4 MPa and a tensile modulus of 3.2 GPa. Elongation at break was 5%. Mix ratio (Part A to Part B) was 100:34.5 by weight.

Six wrap configurations were designed. Three identical specimens for each configuration were prepared and tested to ensure data consistency. Wrap configurations are summarized in Table 2. Each designation is read from left to right, corresponding to the layers from inside out. The number that immediately follows the letter C, meaning cylindrical specimens, shows the total number of wraps used for the specimen. The number that immediately follows any one of the fabric designations (UC, W, or WA) shows the number of plies of that particular type of fabric.

All confined cylinders were wrapped using the wet layup technique after the plain concrete cylinders were primed using thickened epoxy. Proper fabric alignment was visually inspected. A 75 mm lap joint was used and was found to be sufficient from preliminary tests for stress transfer for the given fabric and adhesive systems. A final coat of epoxy was applied to the wrapped specimens for complete saturation. The FRP jackets were then ambient cured for at least 72 h.

Instrumentation and Loading

All specimens were instrumented with extensometers and linear variable differential transducers (LVDTs). Three clip-on extensometers that were mounted 120° apart on the specimens

Table 1. Fiber Reinforced Polymer Fabric Properties

	UC	W	WA
0° (hoop) Tensile strength (MPa)	575.0	309.0	279.0
0° (hoop) Tensile modulus (GPa)	26.1	19.3	18.6
Elongation at break (%)	2.2	1.6	1.5
90° (vertical) Tensile strength (MPa)	21.0	309.0	279.0
Laminate thickness (mm)	1.3	0.3	0.9

Table 2. Wrap Configurations

Configuration	Designation	Description
1	C1-UC1	1 layer of UC fabric
2	C1-W1	1 layer of W fabric
3	C1-WA1	1 layer of WA fabric
4	C2-W1-WA1	1 inner layer of W + 1 outer layer of WA
5	C2-UC1-WA1	1 inner layer of UC + 1 outer layer of WA
6	C2-WA1-UC1	1 inner layer of WA + 1 outer layer of UC

were used to monitor axial strains at mid-height. Two additional vertical LVDT were placed 180° apart close to the cylinders to monitor axial displacements between the loading platens. One of the LVDT was always placed next to the lap joint for referencing. Two specially designed LVDT mounting spring systems, as shown in Fig. 2(a), were mounted 90° apart within

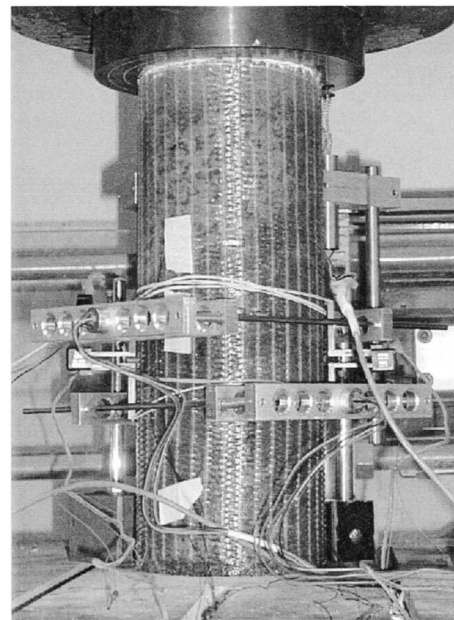
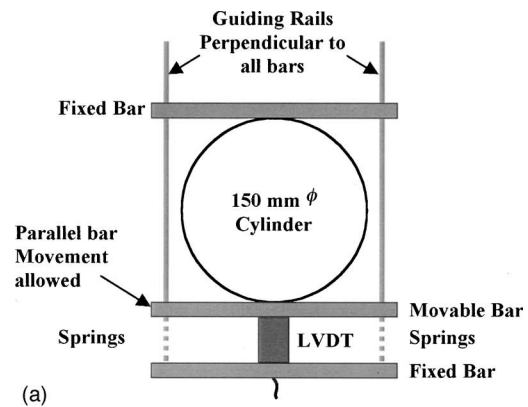


Fig. 2. (a) Linear variable differential transducer mounting spring system and (b) full instrumentation setup

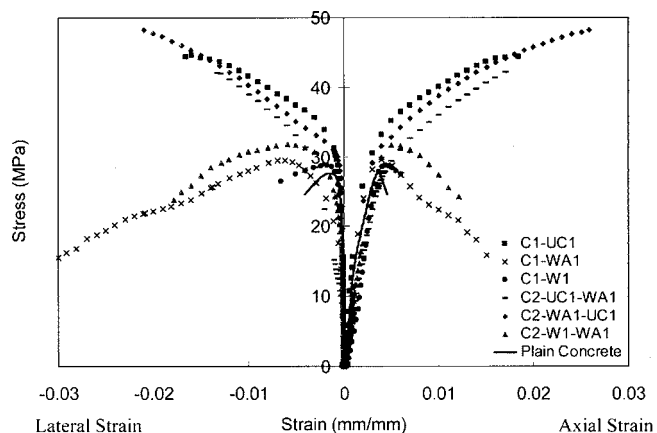


Fig. 3. Selected load–deformation plots of each configuration

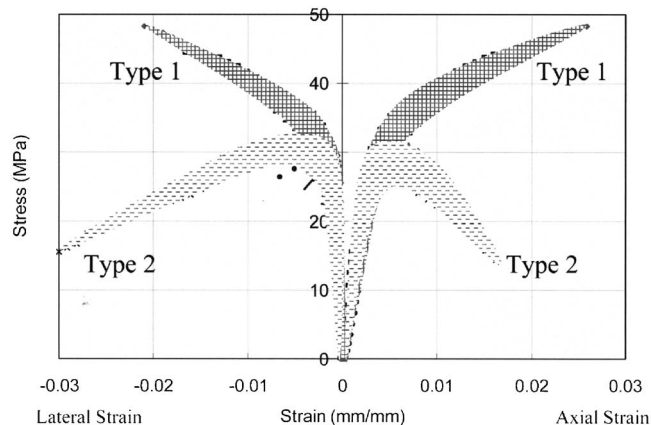


Fig. 4. Banded plots of load–deformation behavior

the 120 mm mid-height range to monitor radial strains in the horizontal plane. A typical full instrumentation setup is shown in Fig. 2(b).

To capture any differential shortening and to simulate realistic joint rotation on top of a column, all cylinders were thinly capped with high strength gypsum at both ends and carefully checked for orthogonality as stipulated in *ASTM C617* (ASTM 2003a), while the top steel platen was set free to rotate. Specimens were tested under monotonic uniaxial compression using a 890 kN Baldwin loading frame in displacement control with a constant rate of 1.25 mm/min.

Test Results

Load–deformation behaviors, which are captured by both axial shortening and radial dilatation, are shown in Fig. 3. For visual clarity, only one set of curves (axial and lateral behavior) that represents a wrap configuration is included in each plot. Each set shown resulted from testing of one specimen. All three tested specimens within each wrap configuration yielded consistent data. Axial strain data used for plotting were obtained from average measurements from the three extensometers for each specimen. Lateral strain data were obtained from average readings for each

specimen from the two spring-loaded lateral LVDT devices. Maximum stress and the associated strains for the respective configurations are summarized in Table 3. Strength increase is computed and ranked.

Observed Load–Deformation Behavior

As observed from Fig. 3, the obtained load–deformation responses consist of two main types. Fig. 4 shows banded plots in which shaded bands are drawn on top of the stress–strain curves shown in Fig. 3 to clearly illustrate the two trends of responses. Note that both single-ply and mixed-ply strengthened specimens could fall within either band.

Type 1 load–deformation demonstrates a system level strain hardening with a distinct bilinear behavior in which a reduction in stiffness is experienced after axial stress has reached a level somewhat higher than the unconfined cylindrical concrete strength. The point at which significant axial stiffness reduction begins is referred to as the kinking point, as termed by Howie (1995). Beyond kinking, there is a steady increase in stress until the wrapped concrete system fails entirely. Failure of Type 1 often involves explosive fiber fracture in the jacket accompanied by concrete crushing in the core. Note also that Type 1 behavior

Table 3. Summary of Peak Stress, Peak Strains, and Strength Increase

Strength rank	Designation	Peak stress average (MPa)	Strain at peak stress average (mm/mm)		Ultimate strength increase average (%)
			Axial	Lateral	
1	C2-WA1-UC1	48.2 (0.55)	0.0260 (0.001021)	0.0221	99
2	C1-UC1	43.8 (0.90)	0.0163 (0.003028)	0.0148	81
3	C2-UC1-WA1	42.6 (3.89)	0.0166 (0.000922)	0.0148	76
4	C2-W1-WA1	31.8 (0.73)	0.0055 (0.000680)	0.0056	32
5	C1-W1	29.8 (1.19)	0.043 (0.001202)	0.0038	23
6	C1-WA1	27.0 (2.83)	0.0050 (0.000922)	0.0076	12
7	Unconfined	24.2 (2.20)	0.0036 (0.000192)	0.0015	—

Note: Standard deviations are indicated as values in parentheses.



Fig. 5. Failure of C1-UC1

always associates with configurations consisting of hoop fibers, which are stiffer and stronger than the other two fiber types used (see Table 1).

Type 2 load–deformation is similar to that of unconfined concrete, except that the peak stress is somewhat higher and that the postpeak straining is much larger as the fractured concrete is contained. A system level strain softening is observed after the peak stress. Note that the peak stress also represents the point at which a change in stiffness occurs. It is termed here the kinking point as well for the purposes of subsequent discussions. Kinking in Type 2 specimens occurs at a somewhat higher level compared to unconfined concrete, but is generally not as high as that in Type 1. Type 2 is seen to associate with bidirectional fibers, which have both lower stiffness and strength than unidirectional fibers in our case. Postpeak straining is particularly pronounced with the use of angular fibers (see Fig. 3). This is demonstrated by the much longer descending tails of the stress–strain curves, signifying a steady decrease in strength without fiber rupture in the jacket. The intact jacket resulted in a high level of physical containment after

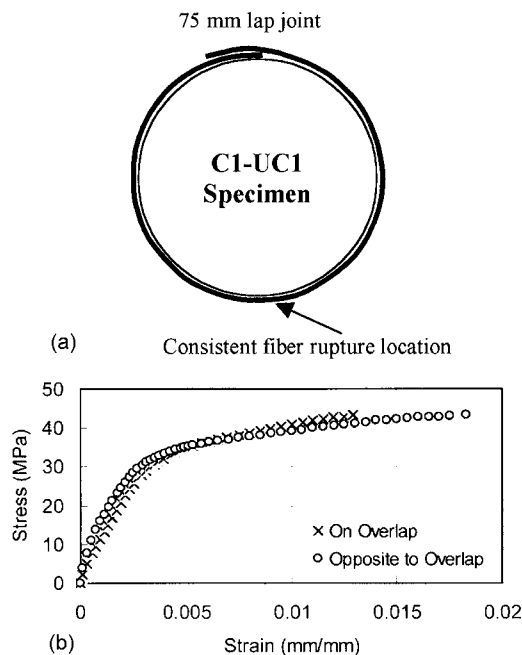


Fig. 6. (a) Fiber rupture location and (b) differential axial shortening

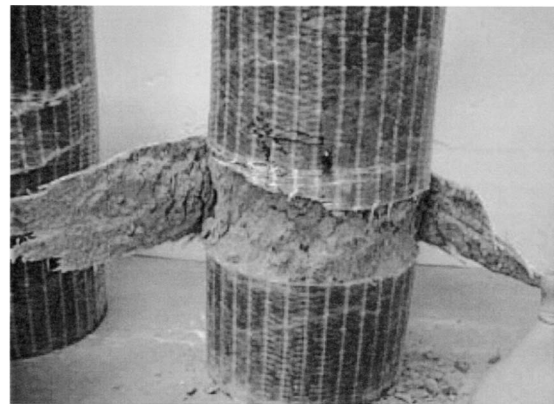


Fig. 7. Localized damage zone of C1-UC1

peak stress is reached, at which fiber reorientation and stretching in the WA fabric started to become obvious. Damaged concrete is well confined until the tests were stopped. Large inclined cracks are, however, seen in the core upon examination after tests. The equivalent fabric stiffness, as computed from the rule of mixtures in laminate theory associated with Type 2, is lower than that in Type 1 regardless of the number of plies. As such, Type 2 behavior is observed with relatively low confinement stiffness.

Observed Failure Modes

At the failure state where system failure was declared by the sudden reduction in load resistance, both brittle and ductile behaviors were observed from the six configurations, although five out of the six showed structural ductility in the form of system-level strain hardening and strain softening before their respective failure points. C1-W1 was the only configuration that did not show ductility during loading and at failure.

Brittle failure state was seen with hoop fiber fracture and hence was associated with all Type 1 load–deformation specimens namely, C1-UC1, C2-UC1-WA1, and C2-WA1-UC1. In addition, C1-W1 also exhibited brittle failure due in part to hoop fiber rupture, as will be discussed in more detail below, although it showed a Type 2 load–deformation behavior. In this case, the fiber rupture was probably due to low fabric strength, which led to jacket failure before further strength enhancing confinement could be developed.

Angular fiber wrap configurations appear to produce a ductile failure state where fiber reorientation occurred in place of fiber fracture that was seen in the case of Type 1. Postpeak straining was substantial both in the axial and radial directions. Tendency of angular fiber reorientation to align with hoop stress direction was noted. This reorientation allowed a relatively compliant radial dilatation, accommodating slippage between cracked concrete inside the containment jacket without rupturing the fibers. This type of failure mode was seen on C1-WA1 and C2-W1-WA1, which both gave rise to Type 2 load–deformation behavior.

Failure of each configuration will be described in detail below under a brittle and ductile failure classification.

Brittle Failure State. *C1-UC1 (One Layer of UC Fabric).* Failure of C1-UC1 was catastrophic and brittle. System failure was registered at peak stress as a result of both fabric fracture and concrete crushing. Fig. 5 shows the failed C1-UC1 specimens. With the top loading platen set free to rotate, differential axial shortening (or bending) was detected, probably due to the local stiffness enhancement in the lap joint area. As a consequence,

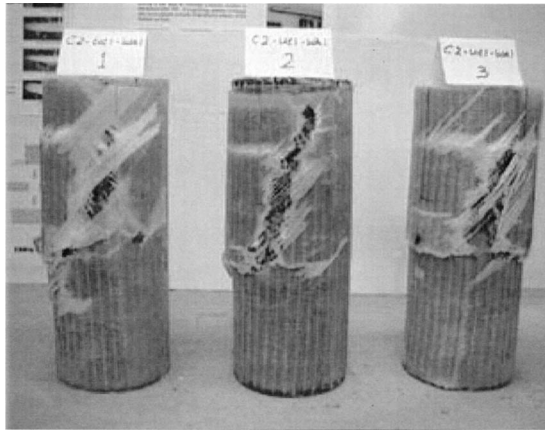


Fig. 8. Failure of C2-UC1-WA1

fiber fracture consistently initiated opposite to the jacket lap joint, as illustrated in Fig. 6(a). This bending behavior was evidenced by the changing orientation of the vertical fibers observed as stress level increased during the test. The resulted differential axial shortening on and opposite to the lap joint was captured by extensometer measurements. A typical axial strain mismatch is shown in Fig. 6(b).

Concrete crushing was highly localized in the mid-height region where bulging was most substantial due to the bending action. Concrete rubbles pushed against the highly strained fabric locally and fractured them when the elastic strain limit of the hoop fibers was reached. Fiber rupture then occurred swiftly and the fabric opened up locally, allowing crushed concrete to spall off, at which state stress level reduced sharply such that complete structural failure was obtained.

Both the concrete core and the FRP jacket above and below the failure region seemed to have remained intact. No major cracking, crushing, or delamination could be found in the top and bottom third except some local whitening at locations where hoop fiber roving and vertical linking fibers crossed, signifying fiber movements under load. A closeup of the damage zone is shown in Fig. 7. Concrete was still adhered to the fractured FRP portion, indicating excellent bonding between the two materials.

C2-UC1-WA1 (One Inner Layer of UC+One Outer Layer of WA). Like C1-UC1, C2-UC1-WA1 failed in a swift and explosive manner. Fig. 8 shows the failed specimens. Failure initiated through fiber fracture in the mid-height region. With the UC lap joint and the WA lap joint set 180° apart, as shown in Fig. 9, the location of crack initiation was not as predictable as in the C1-

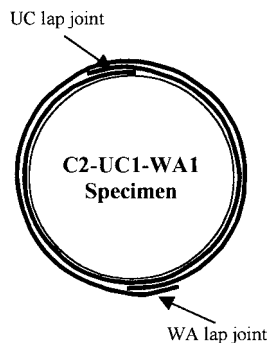


Fig. 9. Balanced lap joint configuration



Fig. 10. Failure of C2-WA1-UC1

UC1 case. It did not simply occur opposite to either lap joint location. Approximately one third to one half of concrete was crushed when fabric fractured open. The crush region was a lot more extensive than in C1-UC1 where only 1 ply of UC fabric was used. Upon disassembly after the test, no distinct global cracking could be identified. Concrete was instead disintegrated into rubbles. Bonding between UC and WA of the fractured fabric was generally intact. Concrete was still adhered to the inner side of the fractured portion, indicating sound bonding between concrete and FRP. Also, failure strains (both axial and radial) of C2-UC1-WA1 were remarkably similar to those in C1-UC1.

C2-WA1-UC1 (One Inner Layer of WA+One Outer Layer of UC). Although the materials used in fabricating C2-UC1-WA1 and C2-WA1-UC1 were identical, the brittle failure took different forms as the stack sequence was reversed, as shown in Fig. 10. Failure of C2-WA1-UC1 was signified by ply delamination between the WA and the UC layer, as shown in Fig. 11. The inner WA layer provided exceptional containment of concrete rubbles up to failure. No concrete spalling was therefore resulted at failure, when UC fabric fractured and delaminated from WA at mid-height. Once fiber fracture was initiated, delamination took place as an accelerated peel action as stress level increased near the ultimate point. Failure was declared when a sudden drop in stress was detected by the feedback loop of the loading frame. From the observation of the failed specimens, the inner WA layer appeared to be intact.

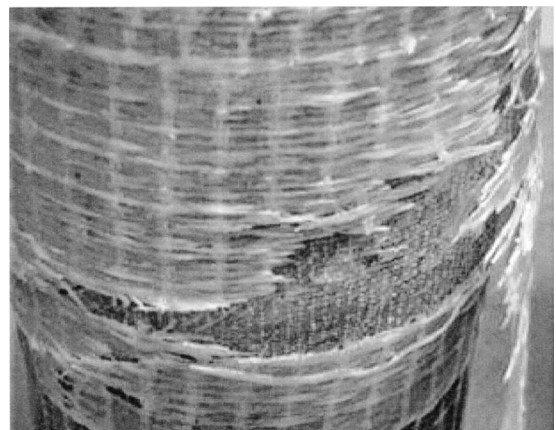


Fig. 11. Delamination between inner WA and outer UC layer

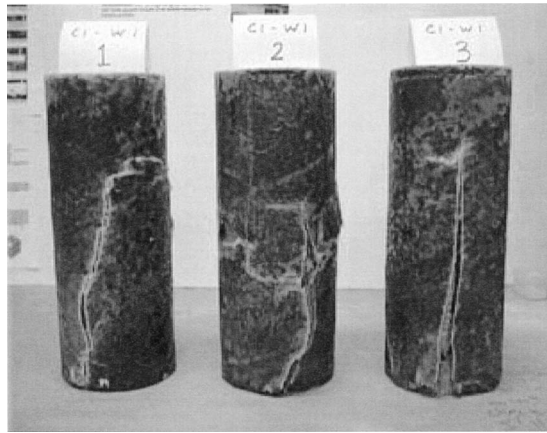


Fig. 12. Failure of C1-W1

C1-W1 (One Layer of W Fabric). C1-W1 exhibited the weakest and most brittle mode among the four within this group. Failed specimens are shown in Fig. 12. The load–deformation appeared to be very close to that of plain concrete, with low axial and radial strains at failure. Failures initiated from one end through local vertical fiber buckling and hoop fiber straining and rupture. The FRP jacket then unzipped upward upon further loading. Upon examination after the test, concrete cracked in a cone-and-split or cone-and-shear manner, similar to that defined in *ASTM C39-03* (ASTM 2003b) for plain concrete. Note that confinement provided by the W jacket was very limited due to its low tensile strength, tensile stiffness, low strain at break, and thinness (see Table 1).

Ductile Failure State. *C1-WA1 (One Layer of WA Fabric).* Failure of C1-WA1 was very ductile, as illustrated by the extensive postpeak straining in Fig. 13. Almost no fiber fracture and concrete spalling could be noted in the postpeak region. This behavior is attributed to the effective containment provided by the WA jacket, which was capable of undergoing large hoop strain by a fiber reorientation mechanism. Fig. 14 shows the local fiber rotation band with a 20° reorientation from the original 45° orientation, trying to align with the stress direction at 0°. Location of the rotation band coincided with the global concrete shear crack developed in the core. Fig. 15 shows a typical shear crack

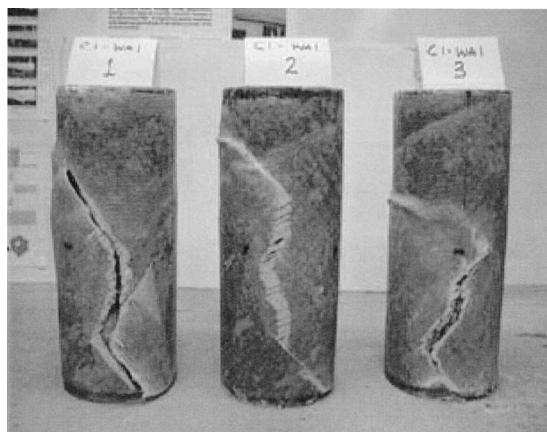


Fig. 13. Failure of C1-WA1

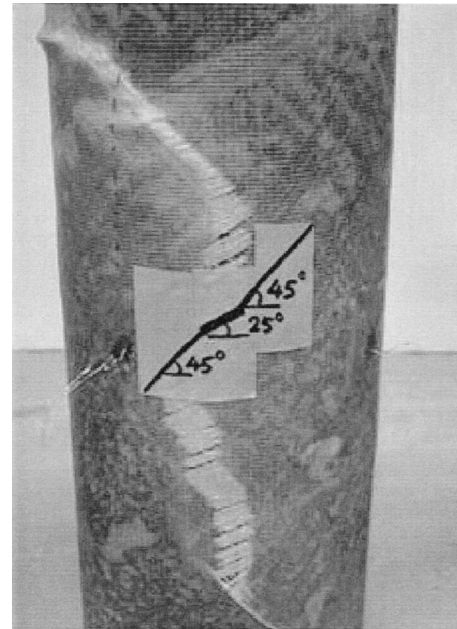


Fig. 14. Fiber reorientation

in C1-WA1 specimens. Note that the jacket was cut open after the test but not ruptured during testing.

C2-W1-WA1 (One Inner Layer of W+One Outer Layer of WA). Failure of C2-W1-WA1 had strong WA dominance with some characteristics of W. As shown in Fig. 16, fiber reorientation took place in the WA jacket, while similar fiber fracture patterns of the W jacket as illustrated in Fig. 12 were also noted. No delamination was noted between the two fabrics. Ductility of C2-W1-WA1 also lie between the fully ductile mode produced by C1-WA1 and the fully brittle mode produced by C1-W1. Upon disassembly, concrete shear cones were also found as in the other two cases.

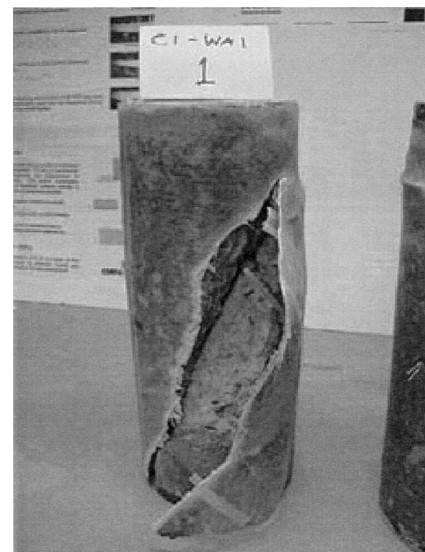


Fig. 15. Global concrete shear crack

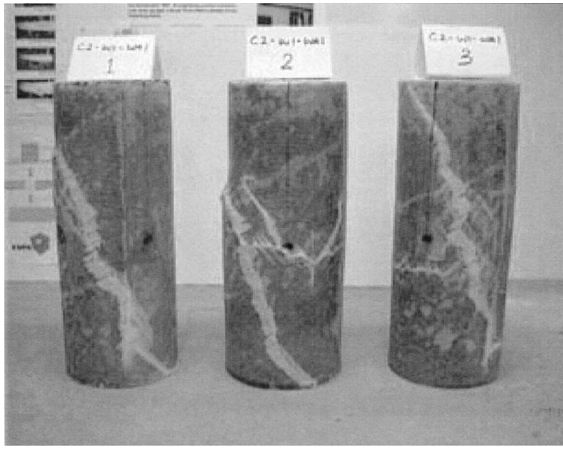


Fig. 16. Failure of C2-W1-WA1

Discussion

Kinking Phenomenon

As discussed earlier, two types of load–deformation behavior beyond kinking can take place—either strain hardening (Type 1) or strain softening (Type 2). In either case, however, a stiffness reduction is experienced as compared to the pre-kinking stiffness. This significant reduction in axial stiffness must imply the failure of concrete core since the FRP jacket still remains intact. Starting from the kink point, further increase in external load results in a more compliant axial behavior. In other words, kinking represents the structural failure of concrete in a cylindrical confined concrete system. In terms of design, the kink stress is of paramount importance. Note that the use of design strength beyond the kink stress for a given jacketed system is yet to be justified, especially for loading cases other than uniaxial compression. As such, there is a need to define precisely the kinking stress level, especially for those jacketed systems that give rise to a transitive kinking region where a clear kink point cannot be easily identified.

Critical Lateral Strain of Concrete and Kink Stress

The definition of the kink stress hinges upon the understanding of the concrete failure behavior in a jacketed system. From a material point of view, concrete splits when the critical lateral strain at a point is reached, regardless of the form of structure it is associated with. For cylindrical plain concrete specimens, failure would take place when a radial strain of 0.001–0.005 is reached (Neville 1973). The material physics should also hold when the concrete specimens are confined. However, the confined concrete system could not reach the critical lateral strain value until a higher axial stress level is attained as a consequence of triaxiality. In other words, the confinement is preventing the specimen from dilating and a higher external axial load is required to achieve the same level of dilatation, and hence kinking. Therefore, a higher confinement pressure would lead to a higher kinking point. Fig. 17 shows the relationship between the critical lateral strain of concrete ϵ_{cr} and the kink stress f_A . This relationship applies well with wrap configurations that exhibited brittle failures.

Effect of Fiber Orientation on Kink Stress

Fiber orientation has a significant effect on the fabric stiffness in the hoop direction in a FRP jacket. The fiber-load alignment deviation is larger and the equivalent fabric stiffness is lower (Peters 1998). A higher jacket stiffness in the hoop direction will result in

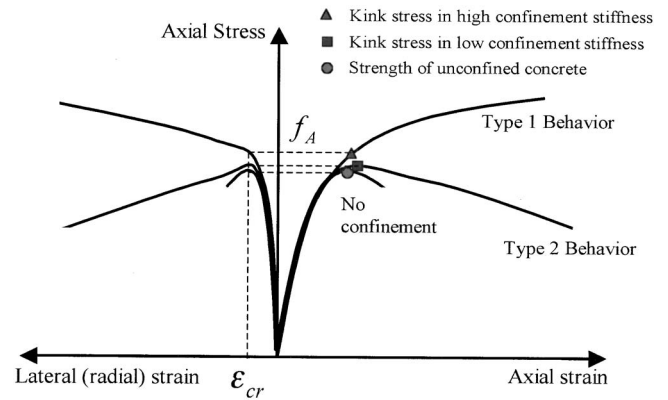


Fig. 17. Relationship between unconfined critical concrete lateral strain and kink stress

a higher confinement pressure and hence a higher kink stress due to the reasons discussed earlier. Assuming that both concrete and FRP materials behave elastically up to the kink stress and that the bond between the two materials is intact, it can be derived from equilibrium and compatibility that the confinement pressure be related to the axial stress as follows:

$$\sigma_p = \nu_c \frac{E_{FRP}(\theta) t_{FRP}}{E_c R} \sigma_a \quad (1)$$

where σ_p = confinement pressure; σ_a = external axial stress; $E_{FRP}(\theta)$ = FRP elastic modulus as a function of θ ; the fiber-hoop stress alignment deviation; t_{FRP} = FRP jacket thickness; E_c = concrete tangent modulus; ν_c = concrete Poisson's ratio; and R = column radius. From the rationale developed before

$$f_A = f(\sigma_p, f'_{co}) \quad (2)$$

where f'_{co} = concrete strength. Hence, f_A is also a function of $E_{FRP}(\theta)$, although the precise relation requires further investigation. But it must be true that a stiffer FRP jacket will give rise to a higher kink stress. In other words, the use of hoop fibers is efficient in upshifting the kink stress level.

Effect of Fiber Orientation on Postkinking Behavior

Beyond kinking, the concrete core has deteriorated. Any additional load will mainly be taken by the FRP jacket in the form of hoop stress. With a similar lateral strain argument as before, the higher jacket stiffness would give rise to stiffer postkinking load–deformation behavior while a stronger jacket would give rise to a higher point of ultimate failure. Since the jacket stiffness and strength are both a function of fiber–load alignment deviation, a higher hoop fiber content would give rise to a stiffer postkinking load–deformation and a higher failure stress. In other words, the use of hoop fibers is effective in promoting stiffer and stronger postkinking behavior. However, this efficiency comes with a serious drawback in terms of failure mode. The FRP composites when loaded in the fiber direction are mostly elastic up to failure. Raising the ultimate state also means that more elastic energy can be released during fiber fracture. The vast amount of elastic energy release thus gives rise to the explosive brittle failure modes, which are contrary to the requirement of structural design.

Angular fibers, on the other hand, seem to be capable of enhancing the overall postkinking ductility of the wrapped column system by means of a fiber reorientation mechanism as seen in Fig. 14. The tendency of fiber–stress alignment yields a safe en-

ergy dissipation mechanism, which leads to a steady stress reduction and excellent rubble containment after the kink stress is reached. The same level of kink stress as high as the hoop fiber confined specimens is also possible by increasing the thickness of the angular fiber jacket, as demonstrated in Eqs. (1) and (2).

For specimens where W fabric was consumed, vertical fibers take up a portion of axial stress through a surface shear transfer mechanism (note that the fiber jackets were not in contact with the loading platen and hence not directly loaded), owing to the intimate bonding between FRP and concrete. With column axial shortening, fiber buckled locally and strained the crossing hoop fibers to rupture, leading to a swift and short postkinking experience.

Effect of Ply Mix

Ply mix generally gave rise to mixed failure and load–deformation behavior (compare Fig. 16 with Figs. 12 and 13) that showed signs of the respective constituent modes. The C2-W1-WA1 exemplified such a mixture effect. The associated load–deformation curves were also bounded between the two extremes, namely C1-W1 and C1-WA1.

Another interesting observation was made between C2-UC1-WA1 and C2-WA1-UC1, of which identical material batches and the same manufacturing and curing procedures were used. Yet, failure modes were so different as evidenced by comparing Figs. 8 and 10. The only possible explanation lies in the different interaction mechanisms between the FRP materials. Fig. 8 shows that two plies could fracture together as one piece in C2-UC1-WA1 while Fig. 11 suggests ply delamination in C2-WA1-UC1.

Note here that UC was a fabric with higher stiffness and strength. Owing to compatibility, the two plies had to undergo the same hoop strain in the postkinking region. However, the stiffer ply would experience a higher stress state at any given time during structural dilatation. Also, WA could exercise fiber reorientation to accommodate large dilatation, as discussed earlier. The UC fabric had to break first even though it possessed a higher strength. In the case of C2-UC1-WA1, with an intimate bond between the FRP plies, the broken UC fibers as the inner layer had no way to release its energy without also breaking the outer layer. Hence, the two plies fractured together explosively (Fig. 8). In the case of C2-WA1-UC1, the higher stressed unconfined UC fibers could fracture upon reaching their strain limits. The only resistance came from the adhesive bonding on the inner side of the UC fabric. But this could be overcome by the elastic energy release during fiber fracture. Hence, the failure modes were completely different, despite the fact that both were brittle.

As such, there seems to be a potential in mixing fabric types to produce better failure modes with more desirable energy dissipation mechanisms such as interply peeling and fiber reorientation by considering the stack sequence of fiber orientation and stiffness.

Comparison of Results with Existing Confinement Models

While the use of angular fibers and/or mix plies has shown some promise in improving ductility during the postpeak state and at the failure state, proper design of such retrofitted cylindrical concrete structures requires accurate modeling of the load–deformation behavior. In this paper, the performance of three representative existing confinement models is therefore evaluated, in view of the findings from this investigation, in order to assess their performance in modeling the stress–strain behavior of such systems.

Karbhari and Gao (1997) developed a model to evaluate the peak confined compressive strength f'_{cc} assuming a bilinear behavior such that

$$f'_{cc} = f_A + f_i \quad (3a)$$

where f_A =kink stress and f_i =stress increment due solely to the confining action when concrete damage has been achieved within the confinement. f_A and f_i are estimated by

$$f_A = f'_{co} + 4.1f'_{co}v_c \left(\frac{E_{FRP}t_{FRP}}{RE_c} \right) \quad (3b)$$

$$f_i = \frac{f_{FRP}t_{FRP}}{R} - f'_{co}v_c \frac{E_{FRP}t_{FRP}}{E_c R} \quad (3c)$$

where f_{FRP} =FRP tensile strength. The ultimate strain, ϵ_{cc} was proposed to be directly dependent on the strength of the FRP such that

$$\epsilon_{cc} = \epsilon_{co} + 0.01 \left(\frac{f_{FRP}t_{FRP}}{Rf'_{co}} \right) \quad (3d)$$

where ϵ_{co} =unconfined peak axial strain of concrete. The researchers however did not propose a stress–strain relationship to describe the entire load–deformation behavior and hence the widely known unified stress–strain model proposed by Mander et al. (1988) was used in this paper. The model relates the confined concrete axial stress f_c with the confined concrete axial strain ϵ_c as follows:

$$f_c = \frac{f'_{cc}x^r}{r-1+x^r} \quad (3e)$$

where

$$x = \frac{\epsilon_c}{\epsilon_{cc}}$$

$$r = \frac{E_c}{E_c - E_{sec}}$$

and

$$E_{sec} = \frac{f'_{cc}}{\epsilon_{cc}}$$

Samaan et al. (1998) developed a bilinear stress–strain model following the four-parameter relationship. The model is expressed as

$$f_c = \left[1 + \left(\frac{(E_1 - E_2)\epsilon_c}{f_A} \right)^n \right]^{1/n} + E_2\epsilon_c \quad (4a)$$

where

$$E_1 = 47.586\sqrt{f'_{co}} \quad (4b)$$

$$E_2 = 52.411(f'_{co})^{0.2} + 2.691(E_{FRP}t_{FRP}/R) \quad (4c)$$

$$f_A = 0.872f'_{co} + 0.371(f_{FRP}t_{FRP}/R) + 0.908 \quad (4d)$$

The ultimate failure state is defined by

$$f'_{cc} = f'_{co} + 3.38 \left(\frac{f_{FRP}t_{FRP}}{R} \right)^{0.7} \quad (4e)$$

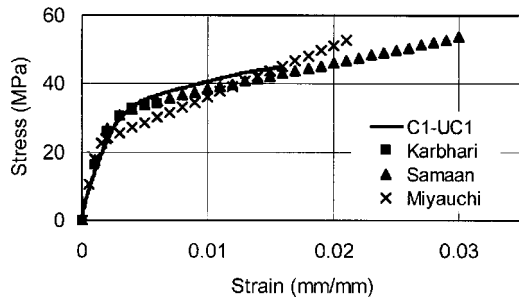


Fig. 18. Experimental and analytical plots (C1-UC1)

$$\varepsilon_{cc} = \frac{f'_{cc} - f_A}{E_2} \quad (4f)$$

Miyauchi et al. (1999) experimentally observed a bi-increasing stress–strain behavior and an increasing–decreasing behavior from hoop fiber wrapped systems with various fiber contents. They thus proposed two different models to describe the respective load–deformation behavior with a clearly defined kinking strain ε_A .

Bi-Increasing Type

For $0 \leq \varepsilon_c \leq \varepsilon_A$

$$f_c = f'_{co} \left(2 \left(\frac{\varepsilon_c}{\varepsilon_{co}} \right) - \left(\frac{\varepsilon_c}{\varepsilon_{co}} \right)^2 \right) \quad (5a)$$

For $\varepsilon_A \leq \varepsilon_c \leq \varepsilon_{cc}$

$$f_c = f'_{cc} - \lambda(\varepsilon_{cc} - \varepsilon_c) \quad (5b)$$

where

$$\lambda = \frac{[-2f'_{co}(\varepsilon_{cc} - \varepsilon_{co}) + \sqrt{4f'_{co}(f'_{co}\varepsilon_{cc}^2 - 2f'_{co}\varepsilon_{co}\varepsilon_{cc} + f'_{cc}\varepsilon_{co}^2)}]}{\varepsilon_{co}^2} \quad (5c)$$

$$\varepsilon_A = \varepsilon_{co} - \frac{\lambda \varepsilon_{co}^2}{2f'_{co}} \quad (5d)$$

$$f_A = f'_{co} \left(2 \left(\frac{\varepsilon_A}{\varepsilon_{co}} \right) - \left(\frac{\varepsilon_A}{\varepsilon_{co}} \right)^2 \right) \quad (5e)$$

Increasing–Decreasing Type

For $0 \leq \varepsilon_c \leq \varepsilon_A$

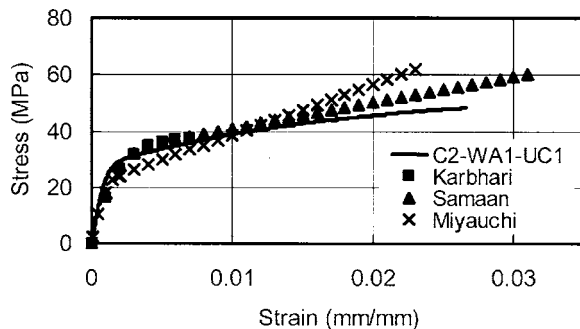


Fig. 19. Experimental and analytical plots (C2-WA1-UC1)

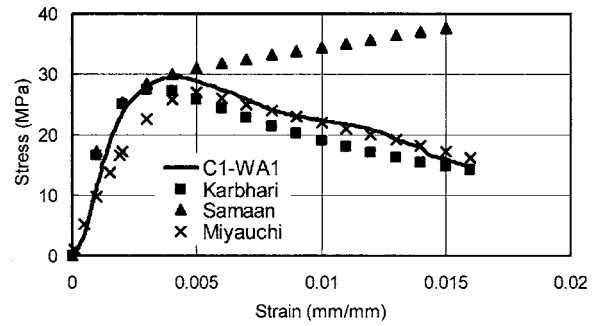


Fig. 20. Experimental and analytical plots (C1-WA1)

$$f_c = f'_{cc} \left(2 \left(\frac{\varepsilon_c}{\varepsilon_{co}} \right) - \left(\frac{\varepsilon_c}{\varepsilon_{co}} \right)^2 \right) \quad (5f)$$

$$f_c = f'_{cc} + \frac{(\varepsilon_c - \varepsilon_{co})(\varepsilon'_{cc} - f'_{co})}{\varepsilon_c - \varepsilon_{co}} \quad (5g)$$

The ultimate compressive capacity is modeled in a similar empirical form as the other researchers as follows:

$$f'_{cc} = f'_{co} + 2.98 \left(\frac{f_{FRP} t_{FRP}}{R} \right) \quad (5h)$$

and the strain at ultimate state is modeled as a nonlinear function as follows:

$$\varepsilon_{cc} = \varepsilon_{co} + \varepsilon_{co} (15.87 - 0.093 f'_{co}) \left(\frac{f_{FRP} t_{FRP}}{R f'_{co}} \right)^{(0.246 + 0.0064 f'_{co})} \quad (5i)$$

Materials data were input into these confinement models to evaluate both Type 1 and Type 2 behaviors. Equivalent FRP properties in the hoop direction computed from laminate mechanics were used. Figs. 18 and 19 show the comparison between representative data sets of Type 1 with the analytical models. It is apparent that the general overall load–deformation behaviors are quite well predicted for the single ply specimen C1-UC1 and the mixed-ply specimen C2-WA1-UC1. All three models predict the kink point relatively well, although the Miyauchi model consistently underestimates the kink stress. While strength prediction is considered adequate, strain predictions do not seem to match well with the experimental findings. In particular, the Karbhari model underestimates the strain at failure in both cases. Figs. 20 and 21 compare the Type 2 behaviors. It is apparent that the Karbhari and Miyauchi models compare favorably with the experimental data while the Samaan model does not represent the descending branch due to the inherent bilinear increasing assumption of the

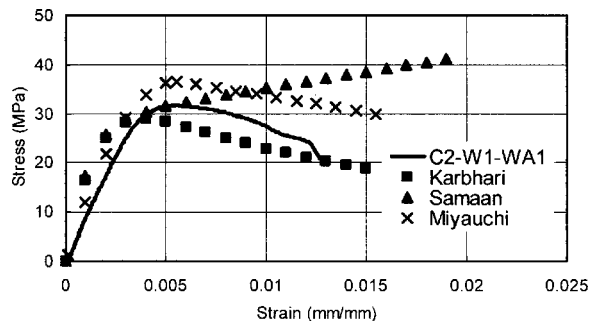


Fig. 21. Experimental and analytical plots (C2-W1-WA1)

model. In particular, the Karbhari model is advantageous in that it utilizes only a single model (of the Mander form) while the Miyauchi model requires assessment of the stress-strain relationship before and after the kink point.

It is clear that the application of these models is generally not affected by the angles of fibers and the ply mix configuration as long as the equivalent FRP hoop properties are used. Also, a bilinear increase assumption does not sufficiently describe the possible range of load-deformation behavior when various fiber wrap configurations are used that result in a range of confinement pressure.

Conclusion

This paper investigates the effects of different fiber orientation and mix of ply configurations on load-deformation behavior and failure modes of FRP confined concrete, with particular emphasis on the kinking phenomenon, which is believed to be a critical physical state from a design standpoint. Within the limitation of the experimental program, the following tentative conclusions have been drawn.

From experimentation, two types of load-deformation behavior were seen on FRP-confined concrete. Type 1, which most often associates with high confinement stiffness and strength, exhibits a system level strain hardening behavior while Type 2, which associates with relatively low confinement properties, shows a system level strain softening behavior. Kinking, which is defined as the point where there is a substantial reduction in axial structural stiffness, signifies structural failure of the concrete core. The kinking point has, in general, a definable graphical relationship with the critical concrete lateral strain. Kink stress appears to shift upward with jacket stiffness and/or thickness. Hoop fibers are efficient in providing confinement, leading to higher kink stress, stiffer postkinking behavior, and higher ultimate failure stress. However, it also yields brittle failure modes with the release of stored strain energy. Angular fiber jackets tend to yield ductile failure modes with its distinct fiber reorientation mechanism to dissipate energy, although they are not mechanically as efficient in strength enhancement. Ply mix tends to give rise to mixed failure mode and load-deformation behavior. Stack sequence also plays an important role in failure behavior. Further studies in stack sequence in terms of fiber orientation and ply stiffness should be made for a better understanding of the energy dissipation mechanisms during failure.

Comparison of experimental results with several representative confinement models has shown that the existing models are generally capable of describing the overall load-deformation of Type 1 behavior, although a bilinear increase assumption would fail to describe the Type 2 behavior. It is also found that the application of these models to quantify angular fiber wrapped systems is generally sufficient when the equivalent FRP properties in the hoop direction are used.

Acknowledgments

The writers acknowledge the support provided, in the form of materials and usage of test facilities, by the Department of Civil and Environmental Engineering of Massachusetts Institute of Technology. Special thanks are also due to Fyfe Co. LLC Ltd. for providing FRP materials and for assistance in jacket installation.

Notation

The following symbols are used in this paper:

- E_c = concrete tangent modulus;
- E_{FRP} = fiber reinforced polymer elastic modulus;
- f_A = kink stress;
- f_c = confined concrete axial stress;
- f'_{cc} = peak confined concrete strength;
- f'_{co} = concrete compressive strength;
- f_{FRP} = tensile strength of fiber reinforced polymer;
- R = column radius;
- t_{FRP} = fiber reinforced polymer jacket thickness;
- ϵ_c = confined concrete axial strain;
- ϵ_{cc} = ultimate confined concrete axial strain;
- ϵ_{co} = critical axial strain of unconfined concrete;
- ϵ_{cr} = critical lateral strain of unconfined concrete;
- θ = fiber-hoop stress alignment deviation;
- ν_c = concrete Poisson's ratio;
- σ_a = external axial stress; and
- σ_p = confinement pressure.

References

- American Society for Testing and Materials (ASTM). (2003a). "Standard practice for capping cylindrical concrete specimens." *ASTM C617*, Philadelphia.
- American Society for Testing and Materials (ASTM). (2003b). "Standard test method for compressive strength of cylindrical concrete specimens." *ASTM C39*, Philadelphia.
- Fyfe Co. LLC (2000). *Design manual for the Tyfo® Fibrwrap® System Rev. 2*.
- Hoppel, C. P. R., and Bogetti, T. A. G. (1997). "Design and analysis of a composite wraps for concrete columns." *J. Reinf. Plast. Compos.*, 16(7), 588–602.
- Howie, I. (1995). "A study on the use of composite wraps for rehabilitation of deteriorated concrete columns." Master thesis, Univ. of Delaware, Newark, Del.
- Howie, I., and Karbhari, V. M. (1995). "Effect of two sheet composite wrap architecture on strengthening of concrete due to confinement: I—Experimental studies." *J. Reinf. Plast. Compos.*, 14, 1008–1030.
- Karbhari, V. M., Eckel, D. A., and Tunis, G. C. (1993). "Strengthening of concrete column stubs through resin infused composite wraps." *J. Therm. Comp. Mat.*, 6, 92–106.
- Karbhari, V. M., and Gao, Y. (1997). "Composite jacketed concrete under uniaxial compression—Verification of simple design equations." *J. Mater. Civ. Eng.*, 9(4), 185–193.
- Lam, L., and Teng, J. G. (2000). "Strength models for FRP-confined concrete." *J. Struct. Eng.*, 128(5), 612–623.
- Mander, J.B., Park, R., and Priestley, M.J.N. (1988). "Theoretical stress-strain model for confined concrete." *J. Struct. Eng.*, 114(8), 1804–1826.
- Mirmiran, A., Kargahi, M., Samaan, M., and Shahawy, M. (1996). "Composite FRP-concrete column, with bi-directional external reinforcement." *Fiber Composites in Infrastructure: Proc., 1st International Conf. in Composites in Infrastructure ICCI'96*.
- Mirmiran, A., and Shahawy, M. (1997a). "Behavior of concrete columns confined by fiber composites." *J. Struct. Eng.*, 123(5), 583–590.
- Mirmiran, A., and Shahawy, M. (1997b). "Dilation characteristics of confined concrete." *Mech. Cohesive-Fract. Mater.*, 2, 237–249.
- Mirmiran, A., Shahawy, M., Samaan, M., Echary, H. E., Mastrapa, J. C., and Pico, O. (1998). "Effect of column parameters on FRP-confined concrete." *J. Compos. Constr.*, 2(4), 175–185.
- Miyauchi, K., Inoue, S., Kuroda, T., and Kobayashi, A. (1999). "Strengthening effects of concrete column with carbon fiber sheet." *Trans. Jpn. Concr. Inst.*, 21, 143–150.

- Nanni, A., and Bradford, N. M. (1995). "FRP jacketed concrete under uniaxial compression." *Constr. Build. Mater.*, 9(2), 115–124.
- Neville, A. M. (1973). *Properties of concrete*, Wiley, New York.
- Peters, S. T., ed. (1998). *Handbook of composites*, 2nd Ed., Chapman and Hall, London.
- Picher, F., Rochette, P., and Labossiere, P. (1996). "Confinement of concrete cylinders with CFRP." *Fiber Composites in Infrastructure: Proc., 1st International Conf. on Composites in Infrastructure*, Tucson, Ariz., 829–841.
- Saadatmanesh, H., Ehsani, M. R., and Li, M. W. (1994). "Strength and ductility of concrete columns externally reinforced with fiber composite straps." *ACI Struct. J.*, 91(4), 434–447.
- Samaan, M., Mirmiran, A., and Shahawy, M. (1998). "Model of concrete confined by fiber composites." *J. Struct. Eng.*, 124(9), 1025–1031.
- van Mier, J. G. M. (1984). "Complete stress-strain behavior and damaging status of concrete under multiaxial conditions." *Proc., RILEM/CEB Symp. on Concrete Under Multiaxial Conditions*, INSA, Toulouse, France.
- Watanabe, K., Nakamura, H., Honda, Y., Toyoshima, M., Iso, M., Fujimaki, T., Kaneto, M., and Shirai, N. (1997). "Confinement effect of FRP sheet on strength and ductility of concrete cylinders under uniaxial compression." *Proc., 3rd International Symp.—Non-Metallic (FRP) Reinforcement for Concrete Structures*, Vol. 1, 233–240.